We are IntechOpen, the world's leading publisher of Open Access books Built by scientists, for scientists

4,800
Open access books available

122,000
International authors and editors

135M
Downloads

Our authors are among the

154
Countries delivered to

TOP 1%
most cited scientists

12.2%
Contributors from top 500 universities

CLARIVATE ANALYTICS BOOK CITATION INDEX INDEXED

WEB OF SCIENCE™

Selection of our books indexed in the Book Citation Index in Web of Science™ Core Collection (BKCI)

Interested in publishing with us?
Contact book.department@intechopen.com

Numbers displayed above are based on latest data collected.
For more information visit www.intechopen.com

17

Optimal Design of a New Wheeled Mobile Robot by Kinetic Analysis for the Stair-Climbing States

Chun-Kyu Woo, Hyun Do Choi, Mun Sang Kim*,
Soo Hyun Kim and Yoon Keun Kwak
Korea Advanced Institute of Science and Technology
** Korea Institute of Science and Technology*
South Korea

1. Introduction

Many mobile robots have been developed in the various application fields, such as building inspection and security, military reconnaissance, space and undersea exploration, and warehouse services (Muir & Neuman, 1987). Mobile robots are designed with the specific locomotive mechanisms according to the environment of the application field. The various locomotive mechanisms used in mobile robots can be classified into three types: wheeled, tracked, and legged type (Kim, 1999) (Lee et al, 2000). Each locomotion type has its inherent advantages and disadvantages as described below. The wheeled mobile robots (WMRs) weigh less than robots of the other locomotive types and have other inherent advantages, such as high energy efficiency, low noise level, etc (Muir & Neuman, 1987). In comparison with legged mobile robots, the WMRs have a simpler driving part and a plain control strategy, but they have the poor adaptability to the terrain.

Tracked mobile robots have the merit of easy off-road travelling. However, they usually have a heavier driving part and need more power for turning motions, in comparison with mobile robots with other locomotive types. Additionally, tracked mobile robots are usually too noisy to be utilized for in-door applications. Legged mobile robots can easily adapt to the unstructured environments, such as off-road environments, but require more actuators to stabilize themselves than mobile robots in the other two categories. As the locomotion mechanisms are complex and need more complicated control algorithms, legged mobile robots have poor mobility on the plane surfaces.

Various types of mobile robots that are capable of climbing up stairs have been developed but, until now, most of the mobile robots developed have tracked-type locomotive mechanisms (Kohler et al., 1976) (Maeda et al., 1985) (Yoneda et al., 1997) (Iwamoto & Yamamoto, 1985) (Iwamoto & Yamamoto, 1990). For the purpose of developing a robot capable of traversing the stairs, Estier (Estier et al., 2000) proposed a WMR with three 4-bar linkage mechanisms, by applying the concept of the instantaneous centre of rotation. To explore Mars, Volpe (Volpe et al., 1997) developed a WMR named Rockey 7, which is capable of climbing up steps about 1.5 times as large as the wheel diameter.

Source: Climbing & Walking Robots, Towards New Applications, Book edited by Houxiang Zhang,
ISBN 978-3-902613-16-5, pp.546, October 2007, Itech Education and Publishing, Vienna, Austria

This paper proposes a new type of locomotive mechanism for WMRs that is capable of travelling up stairs based upon two design concepts: 'adaptability' and 'passivity'. The proposed WMR has a passive linkage-type locomotive mechanism that offers extensive adaptability to rough terrain, especially stair. To fully analyze the behaviours of the proposed passive linkage mechanism during stair climbing, several states analysis was accomplished using the analytical method and the multi-body dynamic analysis software ADAMS™. From the results of the states analysis, the optimization of the proposed WMR was performed using the multi-objective optimization method.

2. The Proposed Locomotive Mechanism

For the purpose of developing a mobile robot which has a simple structure, light weight, and good energy efficiency, we have elaborately analyzed the features of the three types of locomotive mechanism – wheeled, tracked, and legged. The tracked mobile robots have high off-road capability but usually have heavy weight; the tracked mobile robots have low energy efficiency in turning motions; and the legged mobile robots have extensive adaptability to rough terrain but usually have complex locomotive mechanisms that need complicated control algorithms. Additionally, the legged mobile robots have poor mobility on the plane surfaces. On the other hand, the wheeled mobile robots have simple structure, good mobility on the plain surfaces, and good energy efficiency in turning, but have poor adaptability to the rough terrain. Therefore, considering the indoor applications, we opted to develop a wheeled mobile robot. Our wheeled mobile robot, however, has a locomotive mechanism which enables it to adapt to rough terrain, such as the stair like the legged mobile robot.

Therefore, to develop a wheeled mobile robot that not only has adaptability to stairs but also maintains good energy efficiency, we proposed two design concepts. One is adaptability and the other is passivity (Woo et al., 2001). Based on these design concepts, we developed the first prototype of the WMR, named ROBHAZ-6W, and accomplished stair climbing experiments on several types of stairs (Woo et al., 2002). To improve the WMR's adaptability to rough terrain and its ability to climb stairs, this paper presents the modified passive linkage-type locomotive mechanism.

2.1 Adaptability

WMRs usually have been utilized in the indoor environment due to their advantages on the indoor applications. To extend the WMR's application area to the outdoor environment, the WMR must have good adaptability to the environment. In order to improve this adaptability, we proposed a simple linkage-type locomotive mechanism that makes it possible for the driving wheels to move relative to the robot body and for the wheelbases to change among the driving wheels, according to the shape of terrain.

The proposed linkage-type locomotive mechanism is a simple 4-bar linkage mechanism; the side view of the WMR with the proposed mechanism is shown in Fig. 1. As shown in Fig. 1, driving wheels 1 and 2 are interconnected with link 1, which is able to rotate about pin joint P relative to the robot body. Driving wheel 3 is attached to link 2, which is connected with link 1 by pin joint Q. To stabilize the robot body, link 3 is used to connect the robot body to link 2 by pin joints R and S. Therefore, links 1, 2, 3, and the robot body form a 4-bar linkage mechanism which has one degree-of-freedom (DOF). By using the linkage mechanism, the

wheelbases among the driving wheels of the WMR and the relative positions of the wheel axles to the center of gravity of the robot body can be changed, according to the configuration of the proposed linkage-type locomotive mechanism. The WMR has a symmetric structure with the proposed linkage-type locomotive mechanism on the right and the left.

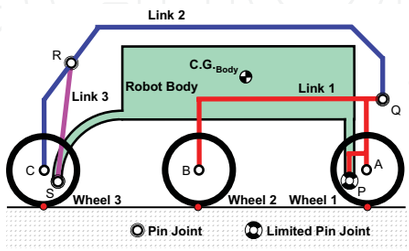

Fig. 1. Side view of the WMR with the proposed linkage-type locomotive mechanism

Fig. 2 shows the adaptability of the WMR with the proposed locomotive mechanism according to the two different types of terrain. As shown in Fig. 2, the 6-WMR with the proposed linkage-type locomotive mechanism easily adapts to the two different types of terrain profile; the concave and the convex terrain. The WMR with the proposed linkage locomotive mechanism has more extensive adaptability to the environment than conventional WMRs. The detailed locomotive method of stair-climbing will be described in the next section.

(a) Concave terrain (b) Convex terrain

Fig. 2. Extensive adaptability of the proposed WMR

2.2 Passivity

As described in the above section, the proposed linkage-type locomotive mechanism offers extensive adaptability to the terrain. Additionally, as shown in Fig. 1, the proposed mechanism does not have any active mechanical elements, such as motors, that need active control techniques. Therefore, the proposed WMR can passively adapt to the environment, according to the linkage-type locomotive mechanism.

However, while the proposed WMR goes up the stairs, the WMR may be led into states which it cannot climb up the stairs and halts where it is. We called these unexpected states 'sticking conditions'. Some of the sticking conditions are shown in Fig. 3.

As shown in Fig. 3 (a), one of the sticking conditions may occur when driving wheels 1 and 2 of the WMR simultaneously come into contact with the wall of the stair. This sticking condition can be evaded by setting the proper wheelbase between driving wheels 1 and 2. Another sticking condition occurs when driving wheels 2 and 3 simultaneously come into contact with the wall of the stair, as shown in Fig. 3 (b). This sticking condition commonly

occurs due to excessive rotation of link 1 relative to the robot body. Not only to avoid this sticking condition and but also to maintain the design concept of 'passivity', we suggested a limited pin joint at point P that restricts the excessive rotation of link 1 relative to the robot body, as described in Fig. 1. The maximum allowable angle of link 1 relative to the robot body will be determined by the kinetic analysis in the next section.

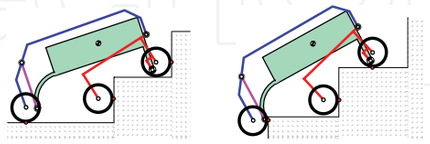

(a) (b)

Fig. 3. Sticking Conditions

3. Kinetic Analysis

In this section, we introduce the detailed analysis of the WMR's states while the WMR with the proposed passive linkage-type locomotive mechanism climbs up the stair. The states are classified in the position of the point and the status of contact between the driving wheels and the stair. The kinetics and the dynamics of the proposed locomotive mechanism at each state are also different from each other due to the posture of the WMR and the contact forces on the driving wheels at the points of contact. The reasons for classifying the climbing motion of the WMR into the several states are to describe the contact forces acting on the driving wheels as the analytic functions and analyze the kinetics of the proposed WMR. For the whole states, the contact forces can not be expressed in the analytic function, due to the absence of contact on certain driving wheels. For each state, however, the normal forces and the corresponding friction forces acting on the driving wheels can be described in the analytic functions.

From the kinetic analysis of each state, the geometric constraints to prevent the WMR from falling into the sticking conditions are suggested and the object functions to improve the WMR's capability to climb up stairs are derived. The design variables of the proposed WMR are shown in Fig. 4.

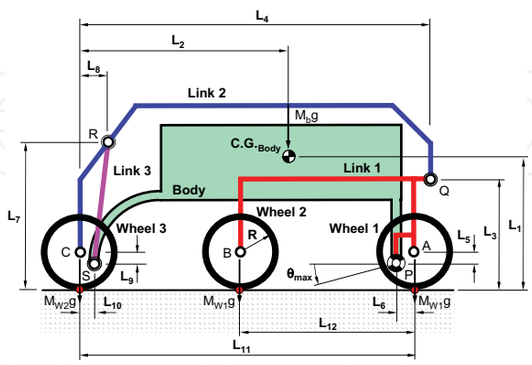

Fig. 4. Design variables of the WMR with the proposed mechanism

The schematic design in Fig. 4 shows the left side of the WMR having a symmetric structure. In Fig. 4, max indicates the maximum allowable counter-clockwise angle of the link 1 at the pin joint relative to the robot body in order to prevent the WMR from falling into the sticking condition.

Fig. 5 shows the suggested 11 states divided by considering the status of the points of contact, while the mobile robot climbs up the stair. In Fig. 5, the small dot attached around the outer circle of the driving wheels indicates the point of contact between the driving wheels and the stair. If the WMR can pass through the whole states, the WMR is able to climb the stair.

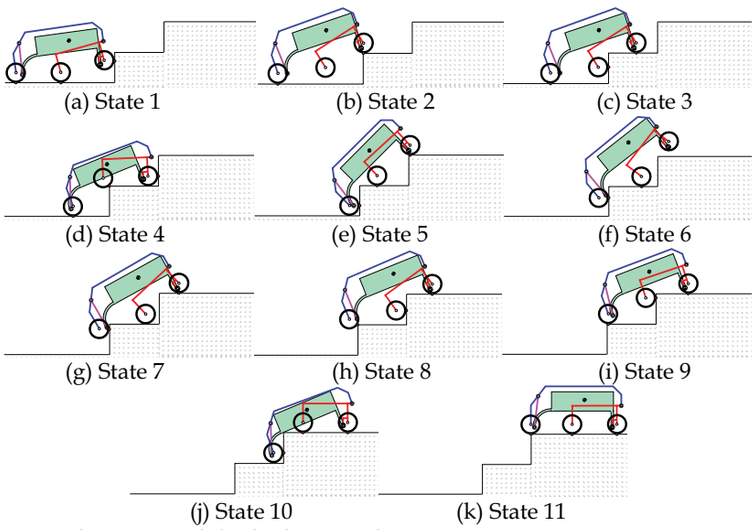

Fig. 5. Suggested 11 states while climbing up the stair

As shown in Fig. 5, the suggested 11 states can be classified into 4 groups. The first group is composed of the states which are kinetically dominant among the whole states, such as states 1, 3, 7, and 10. The capability for the WMR to climb the stair is determined by the states in this group. Therefore, to improve the WMR's ability to climb up the stair, the object functions being optimized will be obtained from the states in this group.

The second group consists of the states that are kinetically analogous to the states in the first group, such as state 4, 8, and 9. State 4 is similar to state 1 in terms of the points of contact between the driving wheels and the stair. States 8 and 9 are analogous to state 2. Therefore, if the object functions obtained from the kinetic analysis of the states in the first group are optimized, it is supposed that the WMR will automatically or easily pass through the states in this group.

The third group comprises the kinematically surmountable states, such as states 5 and 6. In these states, the WMR moves easily to the next state due to the kinematic characteristics of the proposed mechanism.

Finally, the fourth group is formed by the states in which the WMR can be automatically surmountable, such as states 2 and 11. In these states, due to the absence of forces preventing the WMR going forward, the WMR automatically passes through these states.
In the next subsection, we analyze the kinetics of the WMR for the states in the first group by the analytical method. Additionally, using the multi-body dynamic analysis software ADAMS™, we will verify the validity of the kinetic analysis of the WMR. From the results of the kinetic analysis the object functions will be formulated for the purpose of optimizing the design variables of the WMR.

3.1 For State 1

As shown in Fig. 5 (a) and Fig. 6, the driving wheel 1 of the WMR comes into contact with the wall of the stair and driving wheels 2 and 3 keep in contact with the floor, because the center of rotation of the proposed linkage-type mechanism is located below the wheel axis.

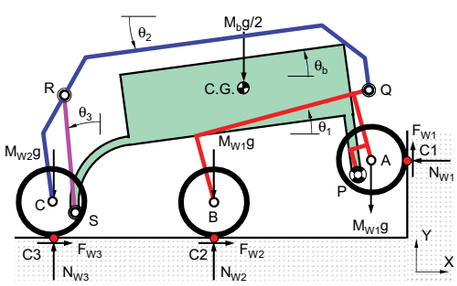

Fig. 6. Forces acting on the proposed WMR for the state 1

To find the normal reaction forces and the corresponding friction forces, we supposed that the WMR was in quasi-static equilibrium and the masses of the links composing the proposed mechanism were negligible. The dynamic friction coefficient of the coulomb friction was applied at the points of contact between the driving wheels and the stair.
If link 1 is in the quasi-static equilibrium state, the resultant forces in the x- and y-directions of the Cartesian coordinates must be zero as described in equation (1) and (2), respectively. The resultant z-direction moment of link 1 about point P also should be zero as described in the equation (3).

$$\sum F_x = 0; \quad \Rightarrow F_{W2} - N_{W1} + P_x + Q_x = 0 \tag{1}$$

$$\sum F_y = 0; \quad \Rightarrow F_{W1} + N_{W2} + P_y + Q_y = 2M_{W1}g \tag{2}$$

$$\begin{aligned} \sum (M_z)_p = 0; \Rightarrow\ & F_{W1}(L_6\cos\theta_1 - L_5\sin\theta_1 + R) + N_{W1}(L_6\sin\theta_1 + L_5\cos\theta_1) \\ & + F_{W2}\{(L_{12} - L_6)\sin\theta_1 - L_5\cos\theta_1 + R\} - N_{W2}\{(L_{12} - L_6)\cos\theta_1 + L_5\sin\theta_1\} \\ & - Q_x\{(L_3 + L_5 - R)\cos\theta_1 + (L_4 + L_6 - L_{11})\sin\theta_1\} \\ & + Q_y\{-(L_3 + L_5 - R)\sin\theta_1 + (L_4 + L_6 - L_{11})\cos\theta_1\} \\ & = M_{W1}g\{(2L_6 - L_{12})\cos\theta_1 - 2L_5\sin\theta_1\} \end{aligned} \tag{3}$$

In equation (3), the forces P_x, P_y, Q_x and Q_y are x- and y-direction joint forces on the point P and Q, respectively. And θ_1 is the counter-clockwise angle of link 1 relative to the x-axis of the coordinates fixed in the ground, as shown in Fig. 6.
For link 2, the x- and y-direction resultant forces are described in equations (4) and (5), respectively. The resultant moment about the point C is expressed in equation (6).

$$\sum F_x = 0; \quad \Rightarrow F_{W3} - Q_x + R_x = 0 \tag{4}$$

$$\sum F_y = 0; \quad \Rightarrow N_{W3} - Q_y + R_y = M_{W2} g \tag{5}$$

$$\begin{aligned} \sum (M_z)_C = 0; \quad \Rightarrow & F_{W3} R + Q_x \{L_4 \sin\theta_2 + (L_3 - R)\cos\theta_2\} - Q_y \{L_4 \cos\theta_2 - (L_3 - R)\sin\theta_2\} \\ & - R_x \{(L_7 - R)\cos\theta_2 + L_8 \sin\theta_2\} - R_y \{(L_7 - R)\sin\theta_2 - L_8 \cos\theta_2\} = 0 \end{aligned} \tag{6}$$

R_x and R_y are x- and y-direction joint forces on the point R, respectively. θ_2 is the counter-clockwise angle of link 2 relative to the x-axis of the coordinates fixed in the ground.
For link 3, the x- and y-direction resultant forces are described in equations (7) and (8), respectively. The resultant moment about point S is expressed in equation (9).

$$\sum F_x = 0; \quad \Rightarrow -R_x + S_x = 0 \tag{7}$$

$$\sum F_y = 0; \quad \Rightarrow -R_y + S_y = 0 \tag{8}$$

$$\sum (M_z)_S = 0; \quad \Rightarrow R_x L \cos\theta_3 + R_y L \sin\theta_3 = 0 \tag{9}$$

S_x and S_y are x- and y-direction joint forces on the point S, respectively. θ_3 is the counter-clockwise angle of link 3 relative to the y-axis of the coordinates fixed in the ground, as shown in Fig. 6. L is the length of link 3 as described in equation (10).

$$L = \left[(L_7 + L_9 - R)^2 + (L_8 - L_{10})^2 \right]^{1/2} \tag{10}$$

Finally, for the robot body, the x- and y-direction resultant forces are described in equations (11) and (12), respectively. The resultant moment about point S is expressed in equation (13).

$$\sum F_x = 0; \quad \Rightarrow -P_x - S_x = 0 \tag{11}$$

$$\sum F_y = 0; \quad \Rightarrow -P_y - S_y = M_b g / 2 \tag{12}$$

$$\begin{aligned} \sum (M_z)_S = 0; \quad \Rightarrow & P_x \{(L_{11} - L_6 - L_{10})\sin\theta_b + (L_9 - L_5)\cos\theta_b\} \\ & - P_y \{(L_{11} - L_6 - L_{10})\cos\theta_b - (L_9 - L_5)\sin\theta_b\} \\ = & \frac{1}{2} M_b g \{(L_2 - L_{10})\cos\theta_b - (L_1 + L_9 - R)\sin\theta_b\} \end{aligned} \tag{13}$$

θ_b is the counter-clockwise angle of the robot body relative to the x-axis of the coordinates fixed in the ground.

The friction force F_{W1} can not be determined by the coulomb friction due to the kinematics of the proposed passive linkage-type locomotive mechanism, but F_{W2} and F_{W3} are determined by the coulomb friction, as in equation (14). These relationships between the normal forces and the friction forces will be shown in the simulation results as described in Fig. 7 where μ represents the dynamic friction coefficient of the coulomb friction.

$$F_{W1} \neq \mu N_{W1}, \quad F_{W2} = \mu N_{W2}, \quad F_{W3} = \mu N_{W3} \tag{14}$$

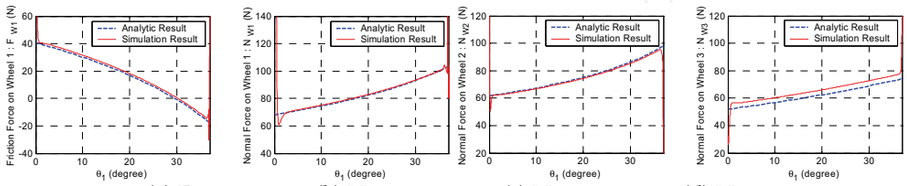

(a) F_{W1} (b) N_{W1} (c) N_{W2} (d) N_{W3}

Fig. 7. Normal and friction forces on the driving wheels for the state 1

From equations (1) ~ (13), we formulate the 12x12 matrix equation as shown in equation (15) to determine the unknown contact forces F_{W1}, N_{W1}, N_{W2} and N_{W3}.

$$\begin{bmatrix} 0 & -1 & \mu & 0 & 1 & 0 & 1 & 0 & 0 & 0 & 0 & 0 \\ 1 & 0 & 1 & 0 & 0 & 1 & 0 & 1 & 0 & 0 & 0 & 0 \\ C_{31} & C_{32} & C_{33} & 0 & 0 & 0 & -C_{37} & C_{38} & 0 & 0 & 0 & 0 \\ 0 & 0 & 0 & \mu & 0 & 0 & -1 & 0 & 1 & 0 & 0 & 0 \\ 0 & 0 & 0 & 1 & 0 & 0 & 0 & -1 & 0 & 1 & 0 & 0 \\ 0 & 0 & 0 & C_{64} & 0 & 0 & C_{67} & -C_{68} & -C_{69} & -C_{610} & 0 & 0 \\ 0 & 0 & 0 & 0 & 0 & 0 & 0 & 0 & -1 & 0 & 1 & 0 \\ 0 & 0 & 0 & 0 & 0 & 0 & 0 & 0 & 0 & -1 & 0 & 1 \\ 0 & 0 & 0 & 0 & 0 & 0 & 0 & 0 & C_{91} & C_{92} & 0 & 0 \\ 0 & 0 & 0 & 0 & -1 & 0 & 0 & 0 & 0 & 0 & -1 & 0 \\ 0 & 0 & 0 & 0 & 0 & -1 & 0 & 0 & 0 & 0 & 0 & -1 \\ 0 & 0 & 0 & 0 & C_{125} & -C_{126} & 0 & 0 & 0 & 0 & 0 & 0 \end{bmatrix} \begin{bmatrix} F_{W1} \\ N_{W1} \\ N_{W2} \\ N_{W3} \\ P_x \\ P_y \\ Q_x \\ Q_y \\ R_x \\ R_y \\ S_x \\ S_y \end{bmatrix} = \begin{bmatrix} 0 \\ 2M_{W1}g \\ M_{W1}gC_{313} \\ 0 \\ M_{W2}g \\ 0 \\ 0 \\ 0 \\ 0 \\ 0 \\ M_bg/2 \\ M_bgC_{1213}/2 \end{bmatrix} \tag{15}$$

The substituted parameters are described.

$$C_{31} = -L_5 \sin\theta_1 + L_6 \cos\theta_1 + R \qquad C_{32} = L_5 \cos\theta_1 + L_6 \sin\theta_1$$
$$C_{33} = -L_5(\mu\cos\theta_1 + \sin\theta_1) + (L_{12} - L_6)(\mu\sin\theta_1 - \cos\theta_1) + \mu R$$
$$C_{37} = (L_3 + L_5 - R)\cos\theta_1 + (L_4 + L_6 - L_{11})\sin\theta_1 \qquad C_{38} = -(L_3 + L_5 - R)\sin\theta_1 + (L_4 + L_6 - L_{11})\cos\theta_1$$
$$C_{313} = -2L_5 \sin\theta_1 + (2L_6 - L_{12})\cos\theta_1 \qquad C_{64} = \mu R$$
$$C_{67} = (L_3 - R)\cos\theta_2 + L_4 \sin\theta_2 \qquad C_{68} = -(L_3 - R)\sin\theta_2 + L_4 \cos\theta_2$$
$$C_{69} = (L_7 - R)\cos\theta_2 + L_8 \sin\theta_2 \qquad C_{610} = (L_7 - R)\sin\theta_2 - L_8 \cos\theta_2$$
$$C_{99} = L\cos\theta_3 \qquad C_{910} = L\sin\theta_3$$
$$C_{125} = (L_{11} - L_6 - L_{10})\sin\theta_b + (L_9 - L_5)\cos\theta_b \qquad C_{126} = (L_{11} - L_6 - L_{10})\cos\theta_b - (L_9 - L_5)\sin\theta_b$$
$$C_{1213} = (L_2 - L_{10})\cos\theta_b - (L_1 + L_9 - R)\sin\theta_b$$

From the 12x12 matrix equation (15), we determined the unknown contact forces as in equations (16) ~ (19).

$$F_{W1} = \begin{bmatrix} \dfrac{(4M_{W1} + M_b)(A1_1 + C_{31}) - 2M_{W1}C_{313} - 2M_{W2}(A1_1 + C_{31} - C_{38})}{2A1_1} g \\ + \dfrac{M_{W2}C_{68}A1_4}{A1_1 A1_2} g - \dfrac{M_b(C_{126} - C_{1213})(C_{37}C_{910} + C_{99}C_{38})}{2A1_1 A1_3} g \\ - \dfrac{M_b(C_{126} - C_{1213})A1_4 A1_5}{2A1_1 A1_2 A1_3} g \end{bmatrix} / 10^3 \tag{16}$$

$$N_{W1} = \begin{bmatrix} - \dfrac{\left[(4M_{W1} + M_b)C_{31} - 2M_{W1}C_{313} - 2M_{W2}(-C_{31} + C_{38})\right]\mu}{2A1_1} g \\ - \dfrac{M_{W2}\mu C_{68}A1_4}{A1_1 A1_2} g + \dfrac{M_b\mu(C_{126} - C_{1213})(C_{910}C_{37} + C_{99}C_{38})}{2A1_1 A1_3} g \\ - \dfrac{M_b\mu(C_{126} - C_{1213})A1_4 A1_5}{2A1_1 A1_2 A1_3} g \end{bmatrix} / 10^3 \tag{17}$$

$$N_{W2} = \begin{bmatrix} - \dfrac{(4M_{W1} + M_b)C_{31} - 2M_{W1}C_{313} - 2M_{W2}(C_{38} - C_{31})}{2A1_1} g \\ + \dfrac{M_{W2}C_{68}}{A1_2} g - \dfrac{M_{W2}C_{68}A1_4}{A1_1 A1_2} g + \dfrac{M_b(C_{126} - C_{1213})A1_5}{2A1_2 A1_3} g \\ + \dfrac{M_b(C_{126} - C_{1213})(C_{99}C_{38} + C_{910}C_{37})}{2A1_1 A1_3} g - \dfrac{M_b(C_{126} - C_{1213})A1_4 A1_5}{2A1_1 A1_2 A1_3} g \end{bmatrix} / 10^3 \tag{18}$$

$$N_{W3} = \left[- \frac{M_{W2}C_{68}}{A1_2} g - \frac{M_b(C_{126} - C_{1213})A1_4}{2A1_2 A1_3} g \right] / 10^3 \tag{19}$$

where,

$$A1_1 = C_{33} - C_{31} + \mu C_{32}, \quad A1_2 = \mu C_{67} - C_{64} - C_{68}$$
$$A1_3 = C_{126}C_{99} + C_{125}C_{910}, \quad A1_4 = C_{33} + \mu C_{37} - C_{38}$$
$$A1_5 = C_{99}C_{610} + C_{68}C_{99} - C_{69}C_{910} + C_{67}C_{910}$$

Here, θ_1, θ_2, θ_3 and θ_b are determined by the kinematics of the proposed mechanism. For this state, θ_2 is a function of θ_1 as described by equation (20) and θ_3 and θ_b are functions of θ_1 and θ_2 as in equations (21) and (22), respectively.

$$\theta_2 = \tan^{-1}\left[\frac{L_4K_1 - (L_3 - R)\left[{L_4}^2 + (L_3 - R)^2 - {K_1}^2\right]^{1/2}}{(L_3 - R)K_1 + L_4\left[{L_4}^2 + (L_3 - R)^2 - {K_1}^2\right]^{1/2}}\right] \tag{20}$$

$$\theta_3 = \tan^{-1}\left[\frac{\left[-2(L_{11} - L_6 - L_{10})M_xM_y + (L_9 - L_5)B_5\right]{B_2}^2 + B_4M_y}{\left[-2(L_9 - L_5)M_xM_y + (L_{11} - L_6 - L_{10})B_6\right]{B_2}^2 + B_4M_x}\right]$$
$$\theta_b = \tan^{-1}\left[\frac{{B_1}^2{B_2}^2B_5 + B_4\left[M_x(L_{11} - L_6 - L_{10}) + M_y(L_9 - L_5)\right]}{B_4\left[M_x(L_9 - L_5) - M_y(L_{11} - L_6 - L_{10})\right]}\right] \tag{21}$$

where,

$$K_1(\theta_1) = (L_3 - R)\cos\theta_1 + (L_4 - L_{11} + L_{12})\sin\theta_1$$
$$M_x(\theta_1, \theta_2) = (L_3 + L_5 - R)\sin\theta_1 - (L_4 + L_6 - L_{11})\cos\theta_1 + (L_4 - L_8)\cos\theta_2 + (L_7 - L_3)\sin\theta_2$$
$$M_y(\theta_1, \theta_2) = -(L_3 + L_5 - R)\cos\theta_1 - (L_4 + L_6 - L_{11})\sin\theta_1 + (L_4 - L_8)\sin\theta_2 - (L_7 - L_3)\cos\theta_2$$
$$B_1 = \left[(L_9 - L_5)^2 + (L_{11} - L_6 - L_{10})^2\right]^{1/2}, \quad B_2 = \left({M_x}^2 + {M_y}^2\right)^{1/2}$$
$$B_3 = -\left(-{M_x}^2 - {M_y}^2 + L^2 + {B_1}^2\right)^2 + 4L^2{B_1}^2$$
$$B_4 = -\left[M_x(L_{11} - L_6 - L_{10}) + M_y(L_9 - L_5)\right]\left(-{B_1}^2 - {B_2}^2 + L^2\right) + \left[M_x(L_9 - L_5) - M_y(L_{11} - L_6 - L_{10})\right]{B_3}^{1/2}$$
$$B_5 = {M_x}^2 - {M_y}^2 - {B_1}^2 + L^2, \quad B_6 = -{M_x}^2 + {M_y}^2 - {B_1}^2 + L^2$$

For this state, the contact forces acting on the driving wheels are described in Fig. 7. The dotted bold lines result from the kinetic analysis as expressed in equations (16) ~ (19) and the solid lines represent the simulation results computed by the multi-body dynamic analysis software ADAMS™.

As shown in Fig. 7, it is allowable to assume that the WMR are in a quasi-static equilibrium. In Fig. 7, the steep changes in the simulation results are caused by the instantaneous collision between driving wheel 1 and the wall of the stair. From Fig. 7 (a) and (b), the

normal force N_{W1} at the point of contact C1 increases as the angle θ_1 of link 1 increases, while the friction force F_{W1} on C1 decreases. Therefore, as shown in equation (14), the coulomb friction does not work between the normal force and the friction force at the point of contact C1. This is due to the kinematics of the proposed linkage-type locomotive mechanism. The other friction forces F_{W2} and F_{W3} on the points of contact C2 and C3 can be determined by the coulomb friction.
For the WMR to be in the equilibrium state, the force F_{W1} can not exceed the friction force produced by the coulomb friction as expressed in equation (22).

$$F_{W1} \le \mu N_{W1} \tag{22}$$

Fig. 8 shows the force difference between N_{W1} and F_{W1}.

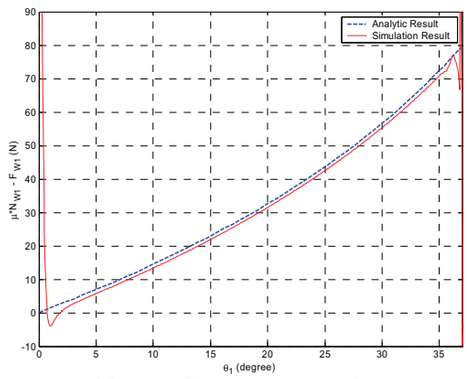

Fig. 8. Force difference between N_{W1} and F_{W1} for the state 1

As shown in Fig. 8, the force difference between N_{W1} and F_{W1} increases as the driving wheel 1 climbs up the stair, that is, as angle θ_1 increases. If the force difference has a negative value, the force F_{W1} must be higher than the coulomb friction N_{W1} that is needed for the WMR to be in the equilibrium state. As shown in equation (22), that situation can not happen absolutely. Therefore, whether the WMR can pass through the state 1 or not is determined at θ_1=0. Consequently, to improve the ability for the WMR to climb up stairs, the force difference at θ_1=0 will be selected as the first object function to be optimized.
The relative angle of link 1 to robot body is limited to avoid sticking conditions described in the previous section. The maximum allowable counter-clockwise angle of link 1 relative to the robot body is expressed in equation (23).

$$\theta_{1b\_\max} = \theta_{1\_\max} - \theta_b\left(\theta_{1\_\max}, \theta_2\left(\theta_{1\_\max}\right)\right),\ where,\ \theta_{1\_\max} = \sin^{-1}\left[\frac{H_{S\_\max} - R}{L_{12}}\right] \tag{23}$$

Here, H_{S_max} is the maximum height of the stair for the WMR to climb and θ_b is determined by equations (20) and (21) at $\theta_1=\theta_{1\_max}$.

3.2 For state 3

In this state, as shown in Fig. 5 (c), driving wheels 1 and 3 of the WMR contact with the floor of the stair and driving wheel 2 comes in contact with the wall of the stair. According to the characteristics of the points of contact, state 3 is divided into two sub-states as shown in Fig. 9. In Fig. 9 (a), the coulomb friction does not work on point of contact C3, while in Fig. 9 (b) the coulomb friction does not function on point of contact C2. This characteristic is due to the kinematic characteristics of the proposed passive linkage-type locomotive mechanism.

3.2.1 For state 3-1

In state 3-1, as shown in Fig. 9 (a), the relative angle of link 1 to the robot body is θ_{1_max} as expressed in equation (23). As mentioned above, the relationships between the normal forces and the friction forces are expressed in equation (24).

$$F_{W1} = \mu N_{W1}, \quad F_{W2} = \mu N_{W2}, \quad F_{W3} \neq \mu N_{W3} \tag{24}$$

In this state, the contact forces can be determined by the same manner as in section 3.1 and as described in equations (25) ~ (28).

$$N_{W1} = \left[\begin{array}{l} \dfrac{(4M_{W1}+M_b)A2_1 - 2M_{W1}D_{313}(D_{64}+D_{67}-\mu D_{68})}{2\left\{\left(1+\mu^2\right)(A2_1+D_{32}D_{68})-(D_{64}+D_{67})A2_2+D_{68}A2_3\right\}}g \\ -\dfrac{M_b(D_{126}+D_{1213})\left\{\begin{array}{l}(\mu D_{38}-D_{32}-D_{37})(A2_5-D_{910}D_{67}) \\ -D_{910}D_{37}(D_{64}+D_{67}-\mu D_{68})+D_{99}A2_1\end{array}\right\}}{2\left\{\left(1+\mu^2\right)(A2_1+D_{32}D_{68})-(D_{64}+D_{67})A2_2+D_{68}A2_3\right\}A2_4}g \end{array} \right] /10^3 \tag{25}$$

$$N_{W2} = \left[\begin{array}{l} \dfrac{\begin{array}{l}(4M_{W1}+M_b)\{\mu(A2_1+D_{32}D_{68})+D_{31}D_{68}\} \\ -2M_{W1}D_{313}\{\mu(D_{64}+D_{67})+D_{68}\}\end{array}}{2\left\{\left(1+\mu^2\right)(A2_1+D_{32}D_{68})-(D_{64}+D_{67})A2_2+D_{68}A2_3\right\}}g \\ +\dfrac{M_b(D_{126}+D_{1213})\left\{\begin{array}{l}(D_{38}+\mu D_{37}-D_{31})A2_5 \\ -D_{99}\{\mu(A2_1+D_{32}D_{68})+D_{31}D_{68}\} \\ +D_{910}\{(\mu D_{64}-D_{68})D_{37}+D_{67}(D_{31}-D_{38})\}\end{array}\right\}}{2\left\{\left(1+\mu^2\right)(A2_1+D_{32}D_{68})-(D_{64}+D_{67})A2_2+D_{68}A2_3\right\}A2_4}g \end{array} \right] /10^3 \tag{26}$$

$$N_{W3} = \left[\begin{array}{l} M_{W2}g - \dfrac{(4M_{W1}+M_b)A2_2(D_{64}+D_{67}) - 2M_{W1}\left(1+\mu^2\right)D_{313}(D_{64}+D_{67})}{2\left\{\left(1+\mu^2\right)(A2_1+D_{32}D_{68})-(D_{64}+D_{67})A2_2+D_{68}A2_3\right\}}g \\ M_bg(D_{126}+D_{1213})\left[\begin{array}{l}-\left(1+\mu^2\right)\left\{\begin{array}{l}(A2_5+D_{68}D_{99}+D_{910}D_{64})D_{37} \\ -D_{38}D_{99}(D_{64}+D_{67})\end{array}\right\} \\ +A2_3(A2_5+D_{68}D_{99}-D_{910}D_{67})\end{array}\right] \\ +\dfrac{}{2\left\{\left(1+\mu^2\right)(A2_1+D_{32}D_{68})-(D_{64}+D_{67})A2_2+D_{68}A2_3\right\}A2_4} \end{array} \right] /10^3 \tag{27}$$

$$F_{W3}=\left[\begin{array}{l}\dfrac{(4M_{W1}+M_b)D_{68}A2_2-2M_{W1}\left(1+\mu^2\right)D_{68}D_{313}}{2\left\{\left(1+\mu^2\right)(A2_1+D_{32}D_{68})-(D_{64}+D_{67})A2_2+D_{68}A2_3\right\}}g \\ +\dfrac{M_b g(D_{126}+D_{1213})\left[\begin{array}{l}\left(1+\mu^2\right)\{D_{38}(A2_5-D_{67}D_{910})+D_{68}D_{37}D_{910}\} \\ -A2_2(A2_5-D_{910}D_{67}+D_{68}D_{99})\end{array}\right]}{2\left\{\left(1+\mu^2\right)(A2_1+D_{32}D_{68})-(D_{64}+D_{67})A2_2+D_{68}A2_3\right\}A2_4}\end{array}\right]/10^3 \quad (28)$$

Here, the substituted parameters are represented below.

$$D_{31}=\mu(R-L_6\sin\theta_1-L_5\cos\theta_1)+(L_6\cos\theta_1-L_5\sin\theta_1)$$
$$D_{32}=-(L_{12}-L_6)(\mu\cos\theta_1+\sin\theta_1)-L_5(\mu\sin\theta_1-\cos\theta_1)+\mu R$$
$$D_{37}=-(L_3+L_5-R)\cos\theta_1-(L_4+L_6-L_{11})\sin\theta_1$$
$$D_{38}=-(L_3+L_5-R)\sin\theta_1+(L_4+L_6-L_{11})\cos\theta_1$$
$$D_{313}=(2L_6-L_{12})\cos\theta_1-2L_5\sin\theta_1 \qquad D_{64}=R$$
$$D_{67}=L_4\sin\theta_2+(L_3-R)\cos\theta_2 \qquad D_{68}=-L_4\cos\theta_2+(L_3-R)\sin\theta_2$$
$$D_{69}=-(L_7-R)\cos\theta_2-L_8\sin\theta_2 \qquad D_{610}=-(L_7-R)\sin\theta_2+L_8\cos\theta_2$$
$$D_{99}=L\cos\theta_3 \qquad D_{910}=L\sin\theta_3$$
$$D_{125}=(L_{11}-L_6-L_{10})\sin\theta_b+(L_9-L_5)\cos\theta_b \qquad D_{126}=-(L_{11}-L_6-L_{10})\cos\theta_b+(L_9-L_5)\sin\theta_b$$
$$D_{1213}=(L_2-L_{10})\cos\theta_b-(L_1+L_9-R)\sin\theta_b$$
$$A2_1=D_{64}D_{38}+D_{67}D_{38}-D_{37}D_{68}-D_{32}D_{68}$$
$$A2_2=\mu D_{32}+D_{31} \qquad A2_3=\mu D_{31}-D_{32}$$
$$A2_4=D_{99}D_{126}-D_{125}D_{910} \qquad A2_5=D_{99}D_{610}-D_{910}D_{69}$$

In this state, the angle of link 2 relative to the x-axis of the coordinates fixed in the ground is expressed in equation (29) due to the kinematics of the proposed mechanism.

$$\theta_2=\tan^{-1}\left[\frac{L_4K_2-(L_3-R)\left[L_4{}^2+(L_3-R)^2-K_2{}^2\right]^{1/2}}{(L_3-R)K_2+L_4\left[L_4{}^2+(L_3-R)^2-K_2{}^2\right]^{1/2}}\right] \quad (29)$$
$$where,\quad K_2(\theta_1)=(L_3-R)\cos\theta_1+(L_4-L_{11})\sin\theta_1+H_s$$

θ_3 and θ_b are determined by equations (20) and (21), respectively. θ_1, θ_2, θ_3, and θ_b are defined by the same manner described in section 3.1.

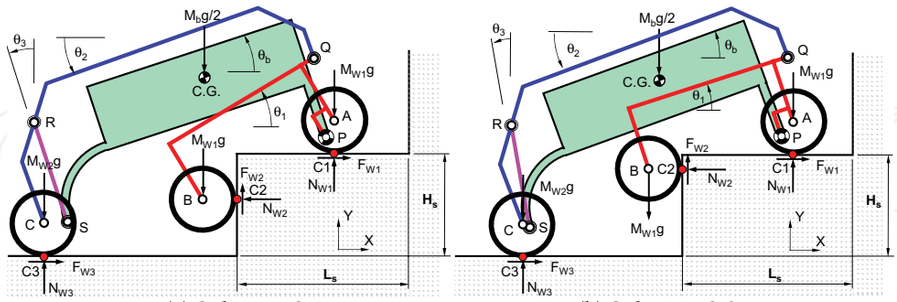

(a) Sub-state 3-1 (b) Sub-state 3-2

Fig. 9. Forces acting on the proposed WMR for the state 3

For this state, the contact forces acting on the driving wheels are described in Fig. 10; the dotted bold lines show the results of the kinetic analysis as expressed in equations (25) ~ (28) and the solid lines represent the simulation results obtained by ADAMS™.

As shown in Fig. 10, it is also allowable to assume that the WMR are in quasi-static equilibrium. In Fig. 10, the steep changes in the simulation results are also caused by the instantaneous collision between the driving wheel 2 and the wall of stair. As shown in Fig. 10 (c) and (d), the coulomb friction does not work between the normal force and the friction force at point of contact C3 as expressed in equation (24). This is also due to the kinematics of the proposed mechanism. The other friction forces F_{W1} and F_{W2} on points of contact C1 and C2 can be determined by the coulomb friction as shown in equation (24).

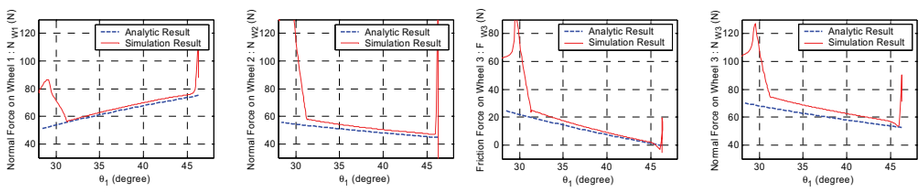

(a) N_{W1} (b) N_{W2} (c) F_{W3} (d) N_{W3}

Fig. 10. Normal and friction forces on the driving wheels for state 3-1

3.2.2 For state 3-2

As link 1 rotates clockwise relative to the robot body, the WMR comes to the state 3-2, as shown in Fig. 9 (b). As mentioned above, the relationships between the normal forces and the friction forces at this state are expressed in equation (30).

$$F_{W1} = \mu N_{W1}, \quad F_{W2} \neq \mu N_{W2}, \quad F_{W3} = \mu N_{W3} \tag{30}$$

In this state, the normal forces and the friction forces can be determined in the same manner as in section 3.1 and as described in equations (31) ~ (34).

$$N_{W1}=\left[\begin{array}{l}-\dfrac{(4M_{W1}+M_b)E_{33}}{2A3_1}g+\dfrac{M_{W1}E_{313}}{A3_1}g+\dfrac{M_{W2}(E_{38}-E_{33})}{A3_1}g-\dfrac{M_{W2}E_{68}}{A3_2}g \\ -\dfrac{M_{W2}E_{68}A3_4}{A3_1A3_2}g-\dfrac{M_bE_{99}E_{38}(E_{126}+E_{1213})}{2A3_1A3_3}g+\dfrac{M_b(E_{126}+E_{1213})A3_5}{2A3_2A3_3}g \\ +\dfrac{M_b(E_{126}+E_{1213})\{A3_4(A3_5+E_{910}E_{67})+E_{910}A3_6\}}{2A3_2A3_2A3_3}g\end{array}\right]/10^3 \quad (31)$$

$$N_{W2}=\left[\begin{array}{l}-\dfrac{(4M_{W1}+M_b)\mu E_{33}}{2A3_1}g+\dfrac{M_{W1}\mu E_{313}}{A3_1}g-\dfrac{M_{W2}\mu E_{68}A3_4}{A3_1A3_2}g \\ +\dfrac{M_{W2}\mu(E_{38}-E_{33})}{A3_1}g-\dfrac{M_b\mu E_{38}E_{99}(E_{126}+E_{1213})}{2A3_1A3_3}g \\ +\dfrac{M_b\mu(E_{126}+E_{1213})\{A3_4(A3_5+E_{67}E_{910})+E_{910}A3_6\}}{2A3_1A3_2A3_3}g\end{array}\right]/10^3 \quad (32)$$

$$F_{W2}=\left[\begin{array}{l}\dfrac{(4M_{W1}+M_b)(\mu E_{32}+E_{31})}{2A3_1}g-\dfrac{M_{W1}E_{313}}{A3_1}g \\ +\dfrac{M_{W2}(\mu E_{32}+E_{31}-E_{38})}{A3_1}g+\dfrac{M_{W2}E_{68}A3_4}{A3_1A3_2}g+\dfrac{M_bgE_{38}E_{99}(E_{126}+E_{1213})}{2A3_1A3_3} \\ -\dfrac{M_b(E_{126}+E_{1213})\{A3_4(A3_5+E_{910}E_{67})+E_{910}A3_6\}}{2A3_1A3_2A3_3}g\end{array}\right]/10^3 \quad (33)$$

$$N_{W3}=\left[\frac{M_{W2}E_{68}}{A3_2}g-\frac{M_b(E_{126}+E_{1213})A3_5}{2A3_2A3_3}g\right]/10^3 \quad (34)$$

Here, the substituted parameters are represented below.

$$E_{31}=\{\mu(R-L_6\sin\theta_1-L_5\cos\theta_1)+(L_6\cos\theta_1-L_5\sin\theta_1)\} \quad E_{32}=-\{(L_{12}-L_6)\sin\theta_1-L_5\cos\theta_1\}$$
$$E_{33}=-\{(L_{12}-L_6)\cos\theta_1+L_5\sin\theta_1-R\} \quad E_{37}=-\{(L_3+L_5-R)\cos\theta_1+(L_4+L_6-L_{11})\sin\theta_1\}$$
$$E_{38}=-\{(L_3+L_5-R)\sin\theta_1-(L_4+L_6-L_{11})\cos\theta_1\} \quad E_{313}=\{(2L_6-L_{12})\cos\theta_1-2L_5\sin\theta_1\}$$
$$E_{64}=\mu R \quad E_{67}=\{L_4\sin\theta_2+(L_3-R)\cos\theta_2\}$$
$$E_{68}=-\{L_4\cos\theta_2-(L_3-R)\sin\theta_2\} \quad E_{69}=-\{(L_7-R)\cos\theta_2+L_8\sin\theta_2\}$$
$$E_{610}=-\{(L_7-R)\sin\theta_2-L_8\cos\theta_2\} \quad E_{99}=L\cos\theta_3 \quad E_{910}=L\sin\theta_3$$
$$E_{125}=\{(L_{11}-L_6-L_{10})\sin\theta_b+(L_9-L_5)\cos\theta_b\} \quad E_{126}=-\{(L_{11}-L_6-L_{10})\cos\theta_b-(L_9-L_5)\sin\theta_b\}$$
$$E_{1213}=\{(L_2-L_{10})\cos\theta_b-(L_1+L_9-R)\sin\theta_b\}$$
$$A3_1=E_{31}+\mu E_{32}-E_{33} \quad A3_2=\mu E_{67}+E_{64}+E_{68}$$
$$A3_3=-E_{99}E_{126}+E_{125}E_{910} \quad A3_4=-E_{31}+\mu E_{37}+E_{38}$$
$$A3_5=E_{68}E_{99}+E_{99}E_{610}-E_{69}E_{910}-E_{910}E_{67} \quad A3_6=E_{67}E_{31}+E_{64}E_{37}-E_{38}E_{67}+E_{68}E_{37}$$

θ_1, θ_2, θ_3, and θ_b are defined in the same manner described in section 3.1. θ_2, θ_3, and θ_b are determined from equations (29), (20) and (21), respectively.

For this state, the contact forces acting on the driving wheels are described in Fig. 11. The dotted bold lines show the results from the kinetic analysis as expressed in equations (31) ~ (34) and the solid lines represent the simulation results by ADAMS™.

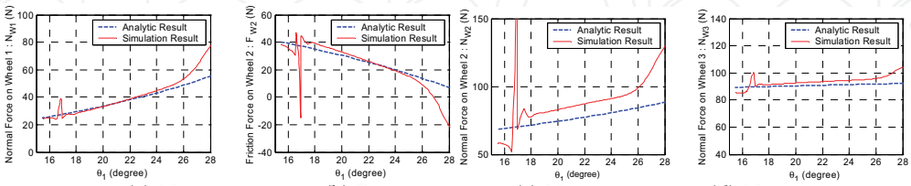

(a) N_{W1} (b) F_{W2} (c) N_{W2} (d) N_{W3}

Fig. 11. Normal and friction forces on the driving wheels for state 3-2

As shown in Fig. 11, it is also allowable to assume that the WMR are in a quasi-static equilibrium. In Fig. 11, the rapid changes in the simulation results are caused by the impact between driving wheel 2 and the wall of the stair. From Fig. 11 (b) and (c), the normal force N_{W2} at point of contact C2 decreases as the angle θ_1 of link 1 decreases, while the friction force F_{W2} on C2 increases. Therefore, as shown in the equation (30), the coulomb friction does not work between the normal force and the friction force at point of contact C2. This is also due to the kinematics of the proposed linkage-type locomotive mechanism. The other friction forces F_{W1} and F_{W3} on points of contact C1 and C3 can be determined by the coulomb friction.

For state 3-1, for the WMR to be in the equilibrium state, the force F_{W3} can not exceed the friction force produced by the coulomb friction as expressed in equation (35).

$$F_{W3} \le \mu N_{W3} \tag{35}$$

Similarly, for state 3-2, the force F_{W2} can not exceed the friction force produced by the coulomb friction as expressed in equation (36).

$$F_{W2} \le \mu N_{W2} \tag{36}$$

Fig. 12 shows the force differences for state 3-1 and the state 3-2. As shown in Fig. 12 (a) and (b), the force difference between N_{W3} and F_{W3} and the force difference between N_{W2} and F_{W2} decrease as driving wheel 2 climbs up the wall of the stair, that is, θ_1 decreases. If equation (36) is satisfied by the design variables of the WMR, equation (35) is satisfied sufficiently for the range of θ_1. Therefore, whether the WMR is able to pass through state 3 is determined when the driving wheel 2 comes in contact with the top-edge of the wall of the step, that is, $\theta_1=\theta_{1\_3}$ as expressed in equation (37). Consequently, to improve the ability of the WMR to climb up the stair, the force difference between N_{W2} and F_{W2} at $\theta_1=\theta_{1\_3}$ will be considered as the second object function.

$$\theta_{1\_3} = \sin^{-1}\left(\frac{R}{L_{12}}\right) \tag{37}$$

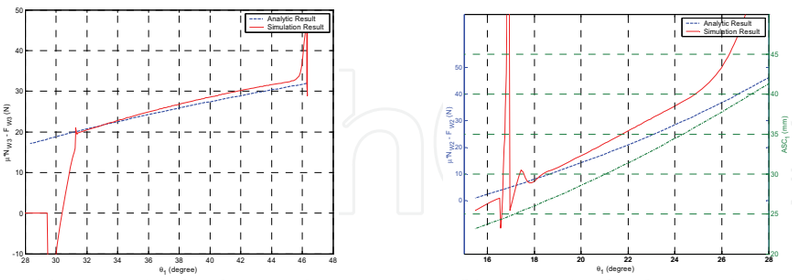

(a) μN_{W3} - F_{W3} for the state 3-1 (b) μN_{W2} - F_{W2} for the state 3-2

Fig. 12. Force differences for the state 3

In Fig. 12 (b), the dash-dotted line represents the distance between the outer circle of driving wheel 1 and the wall of the stair. We call this value the first 'Anti-Sticking Constraint(ASC)'. To prevent the WMR from falling into the sticking condition, the ASC_1 as expressed in equation (38) must be greater than a certain offset value at $\theta_1=\theta_{1\_3}$. The offset value (ASC_{1_off}) is a fully bounded value as described in equation (39). If the ASC_{1_off} increases, the possibility of the sticking condition occurring for this state decreases, even though the WMR climbs the stair with the smaller length than the length of the step L_S.

$$ASC_1 = L_S - L_{12}\cos(\theta_1) \tag{38}$$

$$ASC_1 \geq ASC_{1\_off} \quad where, \quad 0 \leq ASC_{1\_off} \leq R \tag{39}$$

3.2 For State 7

In this state, as shown in the Fig. 5 (g) and Fig. 13, driving wheel 1 comes into contact with the floor of the stair and wheel 3 comes into contact with the wall of the stair. For this state, we assumed that the proposed linkage mechanism has zero degrees-of-freedom. From this assumption, with the exception of the driving wheels, the WMR will move as a rigid body. In this state, the relationships between the normal forces and the friction forces become as found in equation (40).

$$F_{W1} = \mu N_{W1}, \quad F_{W3} = \mu N_{W3} \tag{40}$$

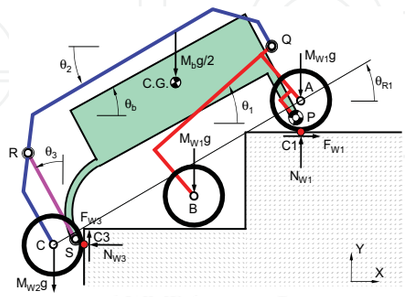

Fig. 13. Forces acting on the proposed WMR for state 7

If the WMR is in a quasi-static equilibrium state, the contact forces can be determined by Newton's 2nd law of motion. The normal forces on points of contact C1 and C3 are determined as described in equations (41) ~ (42).

$$N_{W1} = \left[\frac{(4M_{W1} + 2M_{W2} + M_b)}{2(1+\mu^2)} g \right] / 10^3 \tag{41}$$

$$N_{W3} = \left[\frac{(4M_{W1} + 2M_{W2} + M_b)\mu}{2(1+\mu^2)} g \right] / 10^3 \tag{42}$$

For this state, the contact forces acting on the driving wheels are described in Fig. 14. The dotted bold lines show the results of the kinetic analysis as expressed in equations (41) ~ (42) and the solid lines represent the results by ADAMS™.

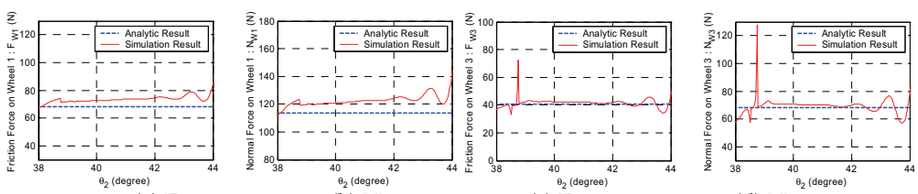

(a) F_{W1} (b) N_{W1} (c) F_{W3} (d) N_{W3}

Fig. 14. Normal and friction forces on the driving wheel 1 and 3 for the state 7

In the simulation results, shown in Fig. 14, the oscillation of the forces is caused by the non-rigid body motion of the proposed linkage mechanism. However, it is allowable to assume that the WMR is in a quasi-static equilibrium and moves as a rigid body.

For the WMR to overcome this state, the z-axis moment acting on the robot about the point of contact C1 must be a negative value (Fig. 13). The z-axis moment about point of contact C1 is expressed in equation (43).

$$\begin{aligned}
(M_z)_{C1} &= \left[-N_{W3}(D_1 + \mu D_2) + M_{W2} g D_3 + M_{W1} g D_4 + M_b g D_5 \right] / 10^3 \\
\textit{where},\ D_1 &= -(L_3 - R)\cos\theta_1 - (L_4 - L_{11})\sin\theta_1 + (L_3 - R)\cos\theta_2 + L_4 \sin\theta_2 - R \\
D_2 &= (L_3 - R)\sin\theta_1 - (L_4 - L_{11})\cos\theta_1 - (L_3 - R)\sin\theta_2 + L_4 \cos\theta_2 - R \\
D_3 &= (L_3 - R)\sin\theta_1 - (L_4 - L_{11})\cos\theta_1 - (L_3 - R)\sin\theta_2 + L_4 \cos\theta_2,\ D_4 = L_{12}\cos\theta_1 \\
D_5 &= -L_5 \sin\theta_1 + L_6 \cos\theta_1 + (L_1 + L_5 - R)\sin\theta_b + (L_{11} - L_2 - L_{10})\cos\theta_b
\end{aligned} \tag{43}$$

Here, θ_1, θ_2, θ_3 and θ_b are described in the equation (44).

$$\begin{aligned} &\theta_1' - \theta_{R1} + \theta_{R2} \le \theta_1 \le \theta_1' \qquad \theta_2' - \theta_{R1} + \theta_{R2} \le \theta_2 \le \theta_2' \\ &\theta_3' - \theta_{R1} + \theta_{R2} \le \theta_3 \le \theta_3' \qquad \theta_b' - \theta_{R1} + \theta_{R2} \le \theta_b \le \theta_b' \\ &where, \quad \theta_{R1} = \sin^{-1}\left[\frac{D_1 + R}{L_R}\right] \qquad \theta_{R2} = \sin^{-1}\left[\frac{H_S + R}{L_R}\right] \end{aligned} \tag{44}$$

Here, θ_1, θ_2, θ_3 and θ_b are described in equation (45) and D_1 is computed from equation (43) when $\theta_1=\theta_1'$ and $\theta_2=\theta_2'$. L_R is the axle length between driving wheels 1 and 3, when the relative angle of link 1 to the robot body is the maximum allowable angle θ_{1b_max} in equation (23), and is computed by equation (46).

$$\begin{aligned} &\theta_1' = \theta_{1\beta} \qquad \theta_2' = \theta_2'' + \theta_{incr} \qquad \theta_3' = \theta_3'' + \theta_{incr} \qquad \theta_b' = \theta_b'' + \theta_{incr} \\ &where, \quad \theta_{incr} = \theta_{1\beta} - \theta_{1\alpha} \qquad \theta_{1\alpha} = \sin^{-1}\left[\frac{H_{S\_\max} - R}{L_{12}}\right] \qquad \theta_{1\beta} = \sin^{-1}\left[\frac{H_S}{L_{12}}\right] \end{aligned} \tag{45}$$

$$L_R = \left[\begin{array}{l} \left\{-(L_3 - R)\sin\left(\theta_2''\right) + L_4\cos\left(\theta_2''\right) - (L_4 - L_{11})\cos(\theta_{1\alpha}) + (L_3 - R)\sin(\theta_{1\alpha})\right\}^2 \\ +\left\{(L_3 - R)\cos\left(\theta_2''\right) + L_4\sin\left(\theta_2''\right) - (L_4 - L_{11})\sin(\theta_{1\alpha}) - (L_3 - R)\cos(\theta_{1\alpha})\right\}^2 \end{array}\right]^{1/2} \tag{46}$$

θ_2", θ_3" and θ_b" are computed from equations (20) and (21) at $\theta_1=\theta_{1\alpha}$, respectively.
For this state, the z-axis moment is described in Fig. 15, according to the change of θ_2. As shown in Fig. 15, from the analytic and simulation results, the z-axis moment increases as driving wheel 3 climbs the wall of the stair, that is, θ_2 decreases. So, for the WMR to climb up the stair, the value of the z-axis moment must be sufficiently less than zero at the moment that driving wheel 3 comes in contact with the top-edge of the wall of the stair.

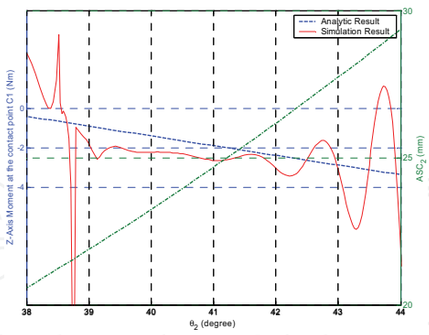

Fig. 15. Z-axis moment about the point of contact C1 for the state 7

In Fig. 15, the dash-dotted line represents the distance between the outer circle of driving wheel 2 and the wall of the stair. We call the value the second 'Anti-Sticking Constraint'. To prevent the WMR from falling into the sticking condition, the ASC_2 as expressed in equation (47) must be greater than a certain offset value (ASC_{2_off}) for all of the range of θ_2. The

ASC_{2_off} is a fully bounded value as described in equation (48). If the ASC_{2_off} increases, the possibility of the sticking condition occurring for this state decreases, even though the WMR climbs the stair with the smaller length than L_S.

$$ASC_2 = L_S - L_4\cos(\theta_2) + (L_3 - R)\sin(\theta_2) + (L_{12} + L_4 - L_{11})\cos(\theta_1) - (L_3 - R)\sin(\theta_1) \quad (47)$$

$$ASC_2 \geq ASC_{2\_off} \quad where, \quad 0 \leq ASC_{2\_off} \leq R \quad (48)$$

Consequently, to optimize the design variables of the proposed WMR, we designate the negative z-axis moment about point of contact C1 at $\theta_2=\theta_{2l}$ as expressed in equation (49) as the third object functions.

$$\theta_{2l} = \theta_2' - \theta_{R1} + \theta_{R2} \quad (49)$$

4. Optimization

In the previous section, we analyzed the kinetics of the WMR with the proposed passive linkage-type locomotive mechanism for several states. From the results of the kinetics, we determined the three object functions to improve the ability of the WMR to climb the stair. Additionally, to prevent the WMR from falling into the sticking conditions as described in section 2, two anti-sticking constraints (ASCs) were described.

In this section, we optimized the design variables of the proposed WMR by using three object functions. The first object function results from the kinetics for state 1 and is described in equation (50). In equation (5), N_{W1} and F_{W1} are computed by equation (16) and (17), respectively. θ_2, θ_3, and θ_b are determined from equations (20) and (21), respectively.

$$OF_1 = \mu N_{W1} - F_{W1}\ , \quad when \quad \theta_1 = 0 \quad \text{for state 1} \quad (50)$$

The second object function results from the kinetics for state 3-2 and represents the force difference between N_{W2} and F_{W2} on point of contact C1 at the moment that driving wheel 2 comes in contact with the top-edge of the wall of the step. This object function is expressed in equation (51). The N_{W2} and F_{W2} are computed from equations (32) and (33), respectively. θ_2, θ_3, and θ_b are determined from equations (29) and (21), respectively.

$$OF_2 = \mu N_{W2} - F_{W2}\ , \quad when\ \theta_1 = \theta_{1\_3} \quad \text{for state 3-2} \quad (51)$$

The third object function results from the kinetics for state 7 and represents the negative z-axis moment on the WMR about the point of contact C1 at the moment that the driving wheel 3 comes in contact with the top-edge of the wall of the step. This object function is described by equation (52) where the normal force N_{W3} and the substituted parameters (D_1, D_2, D_3, D_4 and D_5) are computed from equations (42) and (43), respectively.

$$OF_3 = \left[N_{W3}(D_1 + \mu D_2) - M_{W2}gD_3 - M_{W1}gD_4 - M_bgD_5\right]/10^3 \quad \text{for state 7}$$
$$when\ \theta_1 = \theta_1' - \theta_{R1} + \theta_{R2},\ \theta_2 = \theta_2' - \theta_{R1} + \theta_{R2},\ \theta_3 = \theta_3' - \theta_{R1} + \theta_{R2},\ \theta_b = \theta_b' - \theta_{R1} + \theta_{R2} \quad (52)$$

From the three object functions, we accomplished the optimization of the design variables with the two ASCs as described in equations (38) and (47), respectively, by using the multi-objective optimization method (Gembicki, 1974). The parameters used in the optimization method are listed in Table 1.

Object Functions & Parameters		Values	Object Functions & Parameters		Values
Goal of Object Function	OF_1 (N)	0.3	Dimension of Stair	L_S (mm)	280.0
	OF_2 (N)	1.0		H_S (mm)	165.0
	OF_3 (Nm)	0.3		H_{S_max} (mm)	165.0
ASC_{1_off} (mm)		23.0	ASC_{2_off} (mm)		20.0

Table 1. Object functions and parameters used in the optimization.

The convergence of the three object functions and the optimized design variables, after the optimization process, are showed in Fig. 16 and Table 2, respectively.

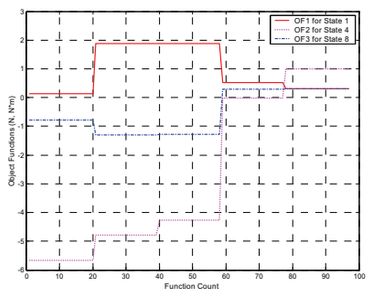

Fig. 16. Convergence of OF_1, OF_2 and OF_3 by the multi-objective optimization method

Design Parameter	Initial Value	Optimal Value	Design Parameter	Initial Value	Optimal Value
L_1 (mm)	160.0	165.0	L_2 (mm)	261.0	263.2
L_3 (mm)	70.0	73.7	L_4 (mm)	455.0	444.6
L_5 (mm)	-40.0	-33.9	L_6 (mm)	40.0	30.7
L_7 (mm)	110.0	112.6	L_8 (mm)	-50.0	-48.0
L_9 (mm)	10.0	12.6	L_{10} (mm)	10.0	8.0
L_{11} (mm)	440.0	425.2	L_{12} (mm)	235.0	225.1
R (mm)	60.0		M_b (kg)	10.9	10.5
M_{W1} (kg)	3.5	3.7	M_{W2} (kg)	2.8	3.2
μ	0.6		OF_1 (N)	0.1	0.3
OF_2 (Nm)	-5.7	1.0	OF_3 (N)	-0.8	0.3

Table 2. The optimal design variables of the proposed WMR

5. Fabrication

Based on the results of optimization, we fabricated the prototype of proposed mobile robot. It is composed mainly of three parts: the driving wheel assembly, the proposed passive linkage mechanism, and the robot body. A motor, a digital encoder, and a harmonic gear are assembled inside the wheel to afford a compact driving unit. The wheel-in motor is shown in Fig. 17.

50Watt Maxon EC flat motors, 500pulse USDigital optical encoders, and 160:1 HarmonicDrive® harmonic gears are used. The passive mechanism is composed of a four bar linkage and a limited pin joint. The pin joint confines the working range of the four bar linkage mechanism to avoid overturning. An electrical subsystem comprised of a single board computer (SBC), a controller area network (CAN) module, a wireless LAN, a motor controller, and Li-ion batteries are placed in the robot body. The prototype of ROBHAZ-6W has eight DOFs: six DOFs for the robot body and two DOFs for the right and left sides of the passive linkage mechanism.

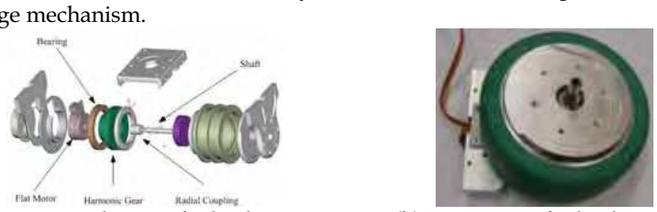

(a) Systematic design of wheel-in motor (b) Prototype of wheel-in motor

Fig. 17. Wheel-in motor

The configurations of the right and left sides of the proposed linkage mechanisms are independently changed according to the environment. And the axle distance between the first and the second driving wheels is determined by considering the length of the stair and the axle distance between the 1st and the 3rd driving wheels is designed according to the height of the stairs that the mobile robot will ascend. The prototype of proposed mobile robot is shown in Fig. 18, and the design parameters are described in Table 3. It can navigate stairs and hazardous terrain areas by using the proposed four bar linkage mechanism.

Item	Parameters	Value	Parameters	Values
Dimensions (mm)	L_1	165.0	L_8	-48.0
	L_2	263.2	L_9	12.6
	L_3	73.7	L_{10}	8.0
	L_4	444.6	L_{11}	425.2
	L_5	-33.9	L_{12}	225.1
	L_6	30.7	R	60.0
	L_7	112.6		
Mass (kg)	Robot Body	10	Wheels & Linkages	18
	Batteries	3	Total	31

Table 3. Design parameters of ROBHAZ-6Wheel

Fig. 19 shows a block diagram of the control system for the robot. This control system is composed of the following: a command PC and a joystick at a remote control site, a single board computer (SBC), six motors and controller, wireless LAN equipment, and a controller
The command PC at the remote site communicates with an SBC in the ROBHAZ-6W. The command PC allows an operator to control the mobile robot movement by joystick and receives angular velocity of wheels by CAN Bus. The motor controllers each have a microprocessor and the six wheel-in motors described in the previous section can be independently controlled. These controllers are connected to the SBC by a CAN bus. This kind of control structure enables the SBC to control the six motors in real time.
All the programs are coded by MS Visual C++ on an MS-Windows 2000 Operating system. The programs are composed of three major parts: a TCP/IP server program, a robot program, and a control program. The TCP/IP server program connects the mobile robot to the remote control PC. The mobile robot program calculates the forward/inverse kinematics of the mobile robot, gives motor driving commands via a CAN bus.

Fig. 18. Prototype of the proposed stair-climbing mobile robot

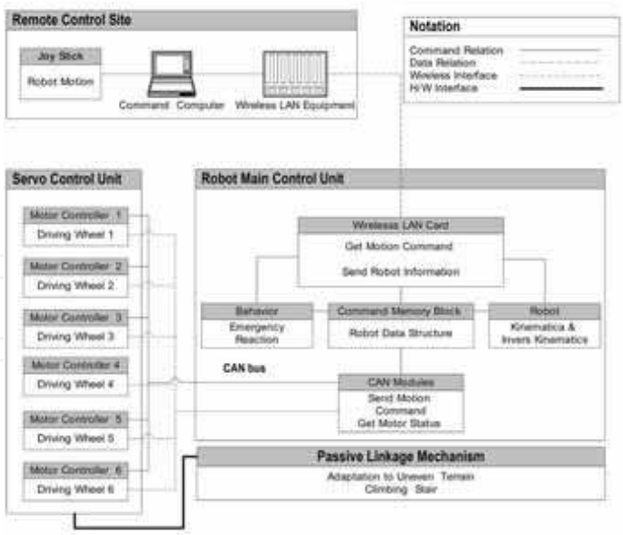

Fig. 19. The full system of proposed mobile robot

6. Experiment

Experimental investigation is performed to prove kinetic analysis and to Fig. out the characteristics of climbing states. We accomplished the experiments with the fabricated stairs of which length and height is 150 mm and 260mm and the indoor stair in KAIST of which length and height is 165 mm and 280mm, respectively. The climbing motions of the fabricated and real stairs are shown in Fig. 20 and Fig. 21, respectively.

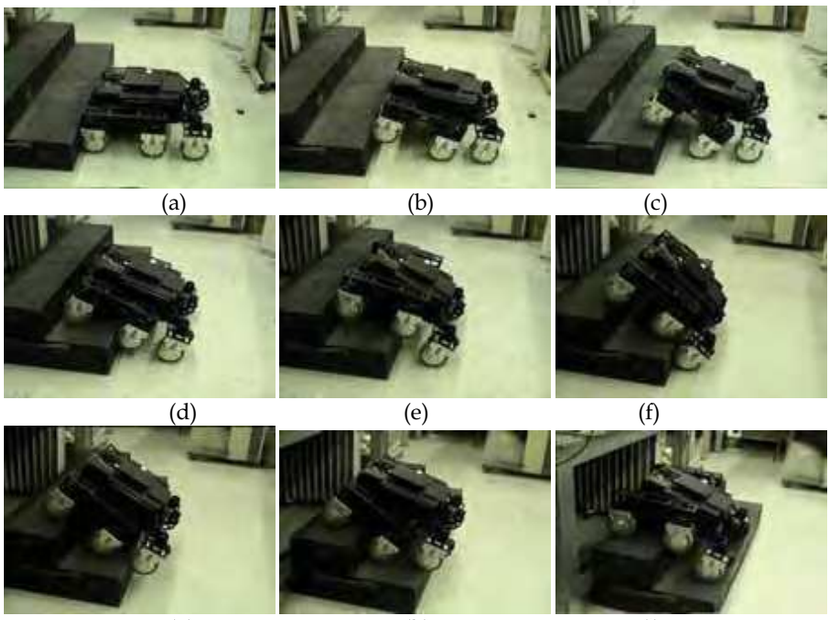

Fig. 20. Experiments for climbing the fabricated stairs

Though the mobile robot is optimized to the stair of which length and height is 165 mm and 280 mm, the proposed mobile robot can easily climb and adapt to the stairs if axle distance is adjusted not to fall in sticking condition.

Table 4 shows the result of adjustment of axle distance to climb the stairs. As L_4 and L_{12} become small, WMR overcome the state1 easily with low friction coefficient. Though WMR has a good ability to overcome state1 with small L_4 and L_{12}, they should not be smaller than specific values which are determined in state 5 and state 7. In state 5 and state 7, there are two important issues which confine minimum length of L_4 and L_{12}. At first, wheel 1 should be in contact with floor of second stair when wheel 3 start climbing up the wall of first stair not to slip on the wall of stair. Second, not to overturn in state 5, L_{12} should be long enough for the contact point of wheel 2 and floor to stay on the right side of WMR's centre of mass.

Fig. 21. Experiments for climbing the real stair

L_4 \ L_{12}	43.5cm	45.5cm	47.5cm
22cm	Overturn (State5)	Overturn (State5)	Overturn (State7)
25cm	Overturn(State5)	Success	Success
28cm	Slipping (State7)	Success	.

Table 4. Climb characteristics in state5 and state7

7. Conclusion

In order to be utilized in building inspection, building security, and military reconnaissance, a new type of WMR was designed with a passive linkage-type locomotive mechanism for improved adaptability to rough terrain and stair-climbing without the active control techniques. Two designed concepts, 'adaptability' and 'passivity', were considered for the design of the linkage-type locomotive mechanism of the WMR. The proposed mechanism, composed of a simple 4-bar linkage mechanism and a limited pin joint, allows the WMR to adapt passively to rough terrain and to climb stairs.

A state analysis was carried out to determine the states that primarily influence the WMR's ability to climb the stair. For the several dominant states suggested from the state analysis, a kinetic analysis was accomplished in order to improve the WMR's ability to climb the stair. The validation of the kinetic analysis was done for the states using ADAMS™. The object functions were formulated from the kinetics of the WMR and we optimized passive link mechanism using the multi-objective optimization method. The proposed WMR with the optimal design values could climb a stair with a height about three times the wheel radius.

8. References

Estier, T.; Crausaz, Y.; Merminod, B.; Lauria, M.; Piguet, R. & Siegwart, R. (2000). *Proc. of Space and Robotics 2000*, Albuquerque, USA, Feb. 27- Mar. 2

Estier, T.; Crausaz, Y.; Merminod, B.; Lauria, M.; Piguet, R. & Siegwart, R. (2000). An Innovative Space Rover with Extended Climbing Abilities, In : *Proc. of Space & Robotics*, the Fourth International Conference and Exposition on Robotics in Challenging Environments, New Mexico

Gembicki, F. W. (1974). *Ph.D. Dissertation*, Case Western Reserve Univ., Cleveland, Ohio

Iwamoto, T. & Yamamoto, H. (1985). *J. of Robotic Systems*, Vol.2 No.1, pp.125-134

Iwamoto, T. & Yamamoto, H. (1990). *J. of Mechanical Design*, Vol.112, pp.289-294

Kohler, G. W.; Selig, M. & Salaske, M. (1976). *Proc. of 24th Conf. on Remote Systems Technology*, pp.196-218

Kim, H. H. (1999). *M.S. Dissertation*, KAIST, Daejeon, Korea

Lee, C. H.; Woo, C. K.; Kim, H. H. & Kwak, Y. K. (2000). *KSAE 2000 Spring Conference*

Maeda, Y.; Tsutani, S. & Hagihara, S. (1985). *Int. Conf. of Robotics and Automation*, pp.421-428

Muir, P. F. & Neuman, C. P. (1987). *J. of Robotic Systems*, Vol.4, No.2, pp.281-340

Volpe, R.; Ohm, T.; Petras, R.; Welch, R.; Balaram, J. & Ivlev, R. (1997). *Proc. of IEEE/RSJ Int. Conf. on Intelligent Robots and Systems*, Grenoble France, Sep. 7-11

Woo, C. K.; Kim, M. S.; Kim, S. H. & Kwak, Y. K. (2001). *Proc. of Int. Conf. on Control, Automation and Systems*, Cheju, Korea, Oct. 17-21, pp.146-149

Woo, C. K.; Cho, C. H.; Kang, S. C.; Shin, K. C.; Kim, M. S.; Kim, S. H. & Kwak, Y. K. (2002). *Proc. of ESDA2002; 6th biennial Conf. on Engineering Systems Design and Analysis*, Istanbul, Turkey, July 8-11

Yoneda, K.; Ota, Y. & Hirose, S. (1997). *J. of Robotic Systems*, Vol.15, No.8, pp.1188-1193

Climbing and Walking Robots: towards New Applications
Edited by Houxiang Zhang

ISBN 978-3-902613-16-5
Hard cover, 546 pages
Publisher I-Tech Education and Publishing
Published online 01, October, 2007
Published in print edition October, 2007

With the advancement of technology, new exciting approaches enable us to render mobile robotic systems more versatile, robust and cost-efficient. Some researchers combine climbing and walking techniques with a modular approach, a reconfigurable approach, or a swarm approach to realize novel prototypes as flexible mobile robotic platforms featuring all necessary locomotion capabilities. The purpose of this book is to provide an overview of the latest wide-range achievements in climbing and walking robotic technology to researchers, scientists, and engineers throughout the world. Different aspects including control simulation, locomotion realization, methodology, and system integration are presented from the scientific and from the technical point of view. This book consists of two main parts, one dealing with walking robots, the second with climbing robots. The content is also grouped by theoretical research and applicative realization. Every chapter offers a considerable amount of interesting and useful information.

How to reference
In order to correctly reference this scholarly work, feel free to copy and paste the following:

Chun-Kyu Woo, Hyun Do Choi, Mun Sang Kim, Soo Hyun Kim and Yoon Keun Kwak (2007). Optimal Design of a New Wheeled Mobile Robot by Kinetic Analysis for the Stair-Climbing States, Climbing and Walking Robots: towards New Applications, Houxiang Zhang (Ed.), ISBN: 978-3-902613-16-5, InTech, Available from: http://www.intechopen.com/books/climbing_and_walking_robots_towards_new_applications/optimal_design_of_a_new_wheeled_mobile_robot_by_kinetic_analysis_for_the_stair-climbing_states

INTECH
open science | open minds

InTech Europe
University Campus STeP Ri
Slavka Krautzeka 83/A
51000 Rijeka, Croatia
Phone: +385 (51) 770 447
Fax: +385 (51) 686 166
www.intechopen.com

InTech China
Unit 405, Office Block, Hotel Equatorial Shanghai
No.65, Yan An Road (West), Shanghai, 200040, China
中国上海市延安西路65号上海国际贵都大饭店办公楼405单元
Phone: +86-21-62489820
Fax: +86-21-62489821

IntechOpen